Orientational order in dipolar fluids consisting of nonspherical hard particles

B. Groh and S. Dietrich
Fachbereich Physik, Bergische Universität Wuppertal, D-42097 Wuppertal, Federal Republic of Germany
(Received 3 September 1996)

We investigate fluids of dipolar hard particles by a certain variant of density-functional theory. The proper treatment of the long range of the dipolar interactions yields a contribution to the free energy which favors ferromagnetic order. This corrects previous theoretical analyses. We determine phase diagrams for dipolar ellipsoids and spherocylinders as a function of the aspect ratio of the particles and their dipole moment. In the nonpolar limit the results for the phase boundary between the isotropic and nematic liquid-crystal phase agree well with simulation data. Adding a longitudinal dipole moment favors the nematic phase. For oblate or slightly elongated particles we find a ferromagnetic liquid phase, which has also been detected in computer simulations of fluids consisting of spherical dipolar particles. The detailed structure of the phase diagram and its evolution upon changing the aspect ratio are discussed in detail. [S1063-651X(97)09402-6]

PACS number(s): 64.70.Md, 61.30.Cz, 77.80.−e,

I. INTRODUCTION

There are two basic molecular properties that can cause long-ranged orientational order in fluids. First, as has already been shown by Onsager [1], particles of sufficiently *anisotropic shape*, e.g., long rods or flat disks, form a nematic liquid-crystal phase at high densities. This phase transition can be induced by purely steric interactions [2–4]. This has been confirmed by computer simulations of hard ellipsoids [5], spherocylinders [6–9], and cut spheres [10,11], which have become standard models of liquid crystals. Some of these systems exhibit further transitions to a smectic or a columnar liquid-crystal phase. Second, there is growing evidence that a ferromagnetically ordered nematic phase can be stabilized by *dipolar interactions* between spherical particles, i.e., in the absence of anisotropic steric interactions. This phase has been observed in Monte Carlo simulations of dipolar soft [12,13] and hard [14–16] spheres as well as in Stockmayer fluids [17]. It has also been analyzed by density-functional theory [18–20]. Due to the long range of the dipolar interactions in this phase the equilibrium configuration exhibits a spatially inhomogeneous magnetization [21], similar to the domain formation in solid ferromagnets.

Molecules typically possess both a shape anisotropy and a permanent dipole moment. Therefore it is interesting to analyze the relative importance of these two properties with respect to the formation of orientationally ordered phases and the crossover from a ferromagnetic to a purely nematic phase. To this end in the present work we study the models of dipolar hard ellipsoids and spherocylinders which cover the models of dipolar hard spheres as well as of nonpolar elongated or oblate hard particles as limiting cases. These models have already been examined by Onsager's virial expansion [22], integral equation theories [23], and different kinds of density-functional theory [24,25]. However, some of these approaches [22,23,25] suffer from an incorrect treatment of the long-ranged dipolar forces and therefore fail to predict a ferromagnetic phase. In simulations of dipolar hard ellipsoids [26] and spherocylinders [27,28,14] and the dipolar Gay-Berne model [29], this phase has also not yet been found, probably because the simulations were restricted to large elongations of the particles which tend to destabilize the ferromagnetic order. Terentjev *et al.* [30] find theoretical indications that a ferromagnetic phase might form more readily in dipolar liquid-crystalline polymers.

In the present work we examine the models mentioned above by an alternative density-functional theory which is a generalization of the theory applied to Stockmayer fluids in Refs. [19–21].

II. DENSITY-FUNCTIONAL THEORY

As motivated in the Introduction, we consider fluids consisting of hard particles which have a symmetry axis and carry in their center a pointlike permanent dipole moment aligned with this axis. The orientation of these uniaxial particles with respect to spatially fixed coordinates is described by two angles $(\theta,\phi)=\omega$. The interaction pair potential $w(\mathbf{r}_{12},\omega,\omega')$ is the sum of the hard core potential and the dipolar potential: $w=w_{hc}+w_{dip}$. The former is given by

$$w_{hc}(\mathbf{r}_{12},\omega,\omega')=\begin{cases}\infty, & r_{12}\leqslant\sigma(\omega_{12},\omega,\omega')\\ 0 & \text{otherwise,}\end{cases} \tag{1}$$

where $\mathbf{r}_{12}=\mathbf{r}-\mathbf{r}'$ is the center-to-center distance vector between the two particles at $\mathbf{r}$ and $\mathbf{r}'$, respectively, and $\sigma(\omega_{12},\omega,\omega')$ is the distance of closest approach for given orientations ω, ω', and ω_{12} of the particle axes and the vector $\mathbf{r}_{12}$, respectively. The dipolar potential has the form

$$\begin{aligned}w_{dip}(\mathbf{r}_{12},\omega,\omega')&=-\frac{m^2}{r_{12}^3}[3[\hat{\mathbf{m}}(\omega)\cdot\hat{\mathbf{r}}_{12}][\hat{\mathbf{m}}(\omega')\cdot\hat{\mathbf{r}}_{12}]\\&\quad-\hat{\mathbf{m}}(\omega)\cdot\hat{\mathbf{m}}(\omega')]\\&=\frac{m^2}{r_{12}^3}\tilde{w}(\omega_{12},\omega,\omega').\end{aligned} \tag{2}$$

In Eq. (2) $\mathbf{m}(\omega)$ is the dipole vector and m is its absolute value. The hats denote unit vectors.

A. Reference system of hard particles

We first analyze the reference system of the corresponding nonpolar hard core fluid. Its free energy as a functional of the number density $\hat{\rho}(\mathbf{r},\omega)$ of particles at $\mathbf{r}$ with orientation ω can be written as

$$F_{ref}=F_{id}+F_{ex}, \tag{3}$$

where the ideal gas part is given by (here and in the following we use the notations $\int d^3r=\int_V d^3r$ and $\int d\omega=\int_{S_2} d\omega$, where V denotes the volume of the sample and S_2 the unit sphere)

$$\beta F_{id}=\int d^3r d\omega \hat{\rho}(\mathbf{r},\omega)\{\ln[4\pi\hat{\rho}(\mathbf{r},\omega)\lambda^3]-1\}, \tag{4}$$

λ being the thermal wavelength. The excess part of the free energy is related to the direct correlation function $c(\mathbf{r},\mathbf{r}',\omega,\omega';[\hat{\rho}])$:

$$-\frac{1}{k_BT}\frac{\delta^2F_{ex}[\hat{\rho}]}{\delta\hat{\rho}(\mathbf{r},\omega)\delta\hat{\rho}(\mathbf{r}',\omega')}=c(\mathbf{r},\mathbf{r}',\omega,\omega';[\hat{\rho}]). \tag{5}$$

Equation (5) can be integrated twice along a linear path in density space starting from a zero density state yielding [31]

$$\begin{aligned}\beta F_{ex}=&-\int d^3r d\omega d^3r' d\omega' \\ &\times\int_0^1 d\lambda(1-\lambda)c(\mathbf{r},\mathbf{r}',\omega,\omega';[\lambda\hat{\rho}]) \\ &\times\hat{\rho}(\mathbf{r},\omega)\hat{\rho}(\mathbf{r}',\omega').\end{aligned} \tag{6}$$

Due to the absence of exact results in order to proceed one now needs an approximation for the direct correlation function. An educated guess, which renders a computationally simple approach but nevertheless yields reliable results for the isotropic-nematic transition of nonpolar hard particles, is given by the decoupling approximation introduced by Pynn [32], which assumes that this anisotropic function can be obtained from a dimensionless function $c_0(x;\eta)$ by a suitable anisotropic rescaling with the distance of closest approach:

$$c(\mathbf{r},\mathbf{r}',\omega,\omega';[\hat{\rho}])\approx c_0(r_{12}/\sigma(\omega_{12},\omega,\omega');\eta). \tag{7}$$

Here $\eta=\rho v^{(0)}$ is the packing fraction of the particles with an individual volume $v^{(0)}$ and $\rho=(1/4\pi V)\int d^3r d\omega\hat{\rho}(\mathbf{r},\omega)$ is the mean number density. In this work we confine ourselves to spatially homogeneous phases so that $\hat{\rho}(\mathbf{r},\omega)=\rho\alpha(\omega)$ with the normalized orientational distribution $\alpha(\omega)$; $\int d\omega\alpha(\omega)=1$. This implies that we do not consider smectic or solid phases and that in the case of ferromagnetic order the sample shape is taken to be needlelike, which suppresses the formation of domains [21]. With these assumptions and approximations Eq. (6) reduces to

$$\frac{\beta F_{ex}}{V}=\rho^2 f_0(\eta)\int d\omega d\omega' d\omega_{12}\alpha(\omega)\alpha(\omega')\sigma^3(\omega_{12},\omega,\omega'). \tag{8}$$

The function c_0 enters only in the integrated form

$$f_0(\eta)=-\int_0^\infty dx x^2\int_0^1 d\lambda(1-\lambda)c_0(x;\lambda\eta). \tag{9}$$

If the Percus-Yevick direct correlation function [33] was used for c_0 one would end up with the Percus-Yevick result for the free energy in the special case of hard spheres [for which obviously $\alpha(\omega)=1/(4\pi)$]. Instead, in accordance with Lee [34,35], we choose

$$f_0(\eta)=\frac{1}{24}\frac{4-3\eta}{(1-\eta)^2}, \tag{10}$$

which follows from the requirement that Eq. (8) yields the Carnahan-Starling expression [36] for the free energy of hard spheres, which is known to be more accurate at high densities. Note that $f_0(\eta)$ does not depend on the shape of the particles which enters Eq. (8) only via the distance $\sigma(\omega_{12},\omega,\omega')$ of closest approach.

In view of the molecular symmetry the orientational distribution $\alpha(\omega)$ is expected to be axially symmetric so that

$$2\pi\alpha(\omega)=\overline{\alpha}(\cos\theta)=\sum_{l=0}^{\infty}\alpha_l P_l(\cos\theta); \tag{11}$$

$P_l(x)$ are the Legendre polynomials. The excluded volume for fixed orientations ω and ω' is given by

$$\begin{aligned}v_{excl}(\omega,\omega')=v_{excl}(\cos\gamma)&=\frac{1}{3}\int d\omega_{12}\sigma^3(\omega_{12},\omega,\omega') \\ &=\sum_{l=0}^{\infty}v_l P_l(\cos\gamma),\end{aligned} \tag{12}$$

where γ denotes the angle between the directions ω and ω'. Insertion of the expansions Eqs. (11) and (12) into Eq. (8) leads to

$$\frac{\beta F_{ex}}{V}=3\rho^2 f_0(\eta)\sum_{l=0}^{\infty}\left(\frac{2}{2l+1}\right)^2 v_l\alpha_l^2. \tag{13}$$

As mentioned above, this expression reduces to the Carnahan-Starling formula in the case of hard spheres. On the other hand, in the limit $\eta\to 0$ one recovers the first two terms of the virial expansion used by Onsager [1]. This limit is especially helpful for very elongated particles for which the isotropic-nematic transition occurs at very low packing fractions.

B. Dipolar interaction

The dipolar contribution to the free energy is treated in the so-called modified mean-field approximation [37–39],

$$\begin{aligned}F_{dip}=&-\frac{\rho^2}{2\beta}\int d^3r d\omega d^3r' d\omega'\alpha(\omega)\alpha(\omega') \\ &\times\Theta(r_{12}-\sigma(\omega_{12},\omega,\omega'))f_{dip}(\mathbf{r}_{12},\omega,\omega'),\end{aligned} \tag{14}$$

with the Mayer function $f_{dip}=\exp(-\beta w_{dip})-1$ which is cut off at contact through the Heaviside function $\Theta(r12$

$-\sigma(\omega_{12},\omega,\omega'))$. This expression follows [38] from using the low-density approximation $g\approx\exp(-\beta w)$ for the pair distribution function. The Mayer function can be expanded as

$$f_{dip}(\mathbf{r}_{12},\omega,\omega')=\sum_{n=1}^{\infty}\frac{1}{n!}\left(\frac{-\beta m^2}{r_{12}^3}\right)^n\tilde{w}^n(\omega_{12},\omega,\omega'). \tag{15}$$

Due to the slow decay as function of r_{12} the first term in this series requires particular attention. For this so-called *long-ranged* term,

$$F_{dip}^{(LR)}=\frac{1}{2}\rho^2\int d\omega d\omega'\alpha(\omega)\alpha(\omega')\int d^3r d^3r' \times\Theta(r_{12}-\sigma(\omega_{12},\omega,\omega'))w_{dip}(\mathbf{r}_{12},\omega,\omega'), \tag{16}$$

the spatial integrations have to be analyzed carefully by first considering a fluid confined to a finite volume V and then performing the thermodynamic limit for a fixed shape of this volume. As has been shown in Ref. [20] the result does depend on the shape of the sample. For an ellipsoidal volume of aspect ratio k it was found that

$$\frac{F_{dip}^{(LR)}}{V}=\frac{8\pi}{9}\rho^2m^2\alpha_1^2(D(k)-1/3)\quad\text{(for spherical particles)}, \tag{17}$$

where $D(k)$ is the demagnetization factor [see Eqs. (3.22) and (3.24) in Ref. [20]]. For nonspherical particles the spatial integrations can be separated into contributions with $r_{12}\leqslant R_c$ and $r_{12}\geqslant R_c$, where R_c is a fixed distance larger than the maximum of $\sigma(\omega_{12},\omega,\omega')$. Since the result in Eq. (17) does not depend on the particle size it can be adopted for the latter contribution ($r_{12}\geqslant R_c$). The remaining integral ($r_{12}\leqslant R_c$) can easily be evaluated since in this case the kernel is effectively short-ranged as function of r_{12}, yielding

$$\frac{F_{dip}^{(LR)}}{V}=\frac{8\pi}{9}\rho^2m^2\alpha_1^2(D(k)-1/3)+\frac{\rho^2}{2\beta}\int d\omega d\omega'\alpha(\omega)\alpha(\omega')q^{(LR)}(\cos\gamma) \tag{18}$$

with

$$q^{(LR)}(\cos\gamma)=\beta m^2\int d\omega_{12}\tilde{w}(\omega_{12},\omega,\omega')\ln\frac{R_c}{\sigma(\omega_{12},\omega,\omega')}=\sum_{l=0}^{\infty}q_l^{(LR)}P_l(\cos\gamma). \tag{19}$$

[As it should be $q^{(LR)}$ does not depend on the arbitrary parameter R_c due to $\int d\omega_{12}\tilde{w}(\omega_{12},\omega,\omega')=0$.] As mentioned above here we consider only the limit of an infinitely long and thin sample ($k\to\infty$) for which $D(k)=0$. For other sample shapes the equilibrium configuration of a ferromagnetic fluid, i.e., with $\alpha_1\neq 0$, exhibits an inhomogeneous structure with a spatially varying axis of preferential orientation, analogouus to the domain formation in solid ferromagnets. It was shown in Ref. [21] that if this effect is taken into account the free energy is independent of the sample shape (see also Ref. [40]) and has the same value as for a spatially homogeneous liquid in the limit $k\to\infty$ and thus the same phase diagram. The other terms in Eq. (14), i.e., the *short-ranged* contributions, can be written in the form

$$\frac{F_{dip}^{(SR)}}{V}=\frac{\rho^2}{2\beta}\int d\omega d\omega'\alpha(\omega)\alpha(\omega')q^{(SR)}(\cos\gamma) \tag{20}$$

with

$$q^{(SR)}(\cos\gamma)=\int d\omega_{12}\sum_{n=2}^{\infty}\frac{(-1)^{n+1}}{3(n-1)n!}\frac{(\beta m^2)^n}{\sigma^{3n-3}(\omega_{12},\omega,\omega')}\times\tilde{w}^n(\omega_{12},\omega,\omega'). \tag{21}$$

With the definition

$$q_l=\frac{2l+1}{2}\int_{-1}^{1}d(\cos\gamma)P_l(\cos\gamma)[q^{(LR)}(\cos\gamma)+q^{(SR)}(\cos\gamma)]-\delta_{l,1}\frac{4\pi}{3}\beta m^2 \tag{22}$$

[$D(k=\infty)=0$] one finally has

$$\frac{\beta F_{dip}}{V}=\frac{1}{2}\rho^2\sum_{l=0}^{\infty}\left(\frac{2}{2l+1}\right)^2q_l\alpha_l^2. \tag{23}$$

C. Total free energy and phase coexistence

Since Eq. (23) has the same form as Eq. (13) we can write the total free energy as in Ref. [20]:

$$\frac{F}{V}=\frac{\rho}{\beta}[\ln(\rho\lambda^3)-1]+\frac{\rho}{\beta}\int_{-1}^{1}dx\,\overline{\alpha(x)}\ln[2\,\overline{\alpha(x)}]+\rho^2\sum_{l=0}^{\infty}u_l\alpha_l^2 \tag{24}$$

with (now density-dependent) coefficients

$$\beta u_l=\left(\frac{2}{2l+1}\right)^2\left[3f_0(\eta)v_l+\frac{1}{2}q_l\right]. \tag{25}$$

If the summation over l is truncated at $l=L$ (in practice it turned out that $L=4$ is sufficient to yield reliable results) the minimization with respect to the orientational distribution leads to

$$\overline{\alpha(x)}\sim\exp\left(-\rho\beta\sum_{i=1}^{L}(\partial i+1)u_i\alpha_iP_i(x)\right) \tag{26}$$

so that [see Eq. (5.6) in Ref. [20]]

$$\alpha_l=\frac{2l+1}{2}\frac{\int_{-1}^{1}dxP_l(x)\exp\left(-\rho\beta\sum_{i=1}^{L}(2i+1)u_i\alpha_iP_i(x)\right)}{\int_{-1}^{1}dx\exp\left(-\rho\beta\sum_{i=1}^{L}(2i+1)u_i\alpha_iP_i(x)\right)}. \tag{27}$$

The phase diagrams follow from requiring the equality of the chemical potentials and the pressures at the coexisting densities ρ_1 and ρ_2:

$$\left.\frac{\partial F}{\partial\rho}\right|_{\rho_1,\overline{\alpha^{(1)}}(x)}=\left.\frac{\partial F}{\partial\rho}\right|_{\rho_2,\overline{\alpha^{(2)}}(x)},$$

$$F(\rho_1,\overline{\alpha^{(1)}}(x))-\rho_1\left.\frac{\partial F}{\partial\rho}\right|_{\rho_1,\overline{\alpha^{(1)}}(x)}=F(\rho_2,\overline{\alpha^{(2)}}(x))-\rho_2\left.\frac{\partial F}{\partial\rho}\right|_{\rho_2,\overline{\alpha^{(2)}}(x)}. \tag{28}$$

The functions $\overline{\alpha^{(l)}}(x)$ denote the corresponding equilibrium orientational distributions obtained from Eqs. (26) and (27). As discussed above, three kinds of phases are considered: isotropic liquid (or gas) [$\overline{\alpha(x)}=1/2$], nematic liquid [$\overline{\alpha(x)}=\overline{\alpha(-x)}$, i.e., $\alpha_l=0$ for odd l], and ferromagnetic liquid ($\alpha_l\neq0$ for all l). (The latter phase could also be called ferromagnetic nematic, but we do not use this phrase in order to avoid confusion.)

The determination of the phase boundaries for *second order* phase transitions is presented in the Appendix. Note that due to symmetry reasons there can be no truly second-order isotropic-nematic transition [41].

We now discuss the calculation of the coefficients v_l and q_l for the two types of particles we are interested in, i.e., hard spherocylinders and hard ellipsoids. A spherocylinder consists of a cylinder of length L and diameter D with two hemispherical caps of the same diameter D. The excluded volume is given by (see, e.g., Ref. [22])

$$v_{excl}(\cos\gamma)=2DL^2\sin\gamma+2\pi D^2L+\frac{4\pi}{3}D^3 \tag{29}$$

which leads to

$$v_0=\frac{\pi}{2}DL^2+2\pi D^2L+\frac{4\pi}{3}D^3,$$

$$v_2=-\frac{5\pi}{16}DL^2,\quad v_4=-\frac{9\pi}{128}DL^2. \tag{30}$$

(Higher-order terms are neglected.) The odd coefficients vanish due to the presence of the symmetry plane of the (nonpolar) particles. In order to determine the coefficients q_l one needs the function $\sigma(\omega_{12},\omega,\omega')$. It can be inferred from the observation that the surface of a spherocylinder is the set of all points with distance $D/2$ from the line segment connecting the centers of the caps. Thus when two spherocylinders are in contact these line segments always have the distance D from each other. It is difficult to give a closed formula for $\sigma(\omega_{12},\omega,\omega')$ because several cases have to be distinguished. Nonetheless a numerical code for the calculation of this function can easily be implemented. An algorithm for the closely related problem of the distance between two spherocylinders with given positions and orientations has been derived explicitly by Allen *et al.* [4].

For hard ellipsoids with two equal axes of length $\sigma_\perp$ and one axis of length $\sigma_\parallel$ Berne and Pechukas [42] introduced the often used approximation [31]

$$\sigma(\omega_{12},\omega,\omega')=\sigma_\perp\left[1-\chi\frac{\cos^2\theta+\cos^2\theta'-2\chi\cos\theta\cos\theta'\cos\gamma}{1-\chi^2\cos^2\gamma}\right]^{-1/2} \tag{31}$$

where γ, θ, and θ' are the angles between the directions ω and ω', ω and ω_{12}, and ω' and ω_{12}, respectively, and

$$\chi=\frac{\sigma_\parallel^2-\sigma_\perp^2}{\sigma_\parallel^2+\sigma_\perp^2}=\frac{\kappa^2-1}{\kappa^2+1}; \tag{32}$$

$\kappa=\sigma_\parallel/\sigma_\perp$. This approximation is obtained by considering the overlap of two ellipsoidal Gauss distributions. From Eq. (31) one finds

$$v_{excl}(\cos\gamma)=\frac{4\pi}{3}\sigma_\parallel\sigma_\perp^2\left(\frac{1-\chi^2\cos^2\gamma}{1-\chi^2}\right)^{1/2}. \tag{33}$$

These formulas enable one to determine the coefficients v_l analytically and q_l numerically. We have truncated the sum in Eq. (21) at $n=30$ and found no significant changes upon including further terms for all considered values of the parameters βm, $\sigma_\parallel/\sigma_\perp$, and D/L.

III. DISCUSSION OF THE PHASE DIAGRAMS

A. Nonpolar ellipsoids

Figure 1 displays the phase diagram for *nonpolar* hard ellipsoids with aspect ratio $\kappa=\sigma_\parallel/\sigma_\perp$. The solid lines denote the coexistence densities of the isotropic and the nematic fluid as determined from the theory presented in Sec. II. They are in fair agreement with the results of Monte Carlo simulations (squares) [5]. The two-phase region is always very narrow, as in real nematic liquid crystals. The triangles indicate the liquid-solid transition found in the simulations, which cannot be described by the present theory. (The description of the solid phase requires a weighted-density-functional theory [43].) For aspect ratios near $\kappa=1$ the isotropic-nematic transition is preempted by freezing. Within the approximation in Eq. (31) the physical properties are invariant under the transformation $\kappa\to1/\kappa$. This behavior is satisfied very well by the simulation results, too.

B. Polar ellipsoids

In this section we discuss the case that the hard ellipsoids are endowed with a point dipole of strength m oriented along the symmetry axis of length $\sigma_\parallel$. In the following we use the dimensionless reduced temperature $T^*=k_BT\sigma_\perp^3/m^2$ and the volume fraction $\eta=\rho v^{(0)}$ where $v^{(0)}=(\pi/6)\sigma_\perp^2\sigma_\parallel$ is the mo-

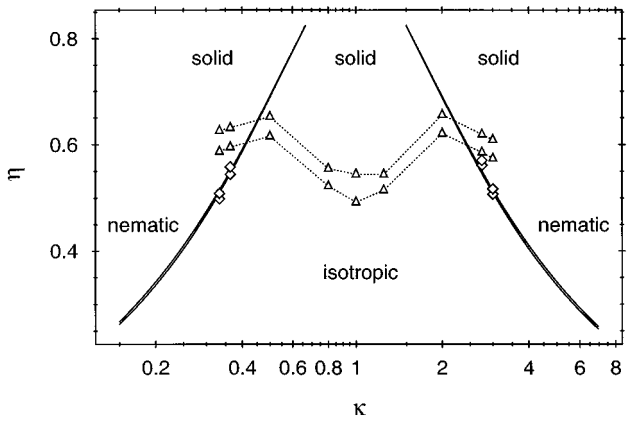

FIG. 1. Phase diagram of nonpolar hard ellipsoids with two equal axes of length $\sigma_\perp$ and one axis of length $\sigma_\parallel$ and an aspect ratio $\kappa=\sigma_\parallel/\sigma_\perp$. $\eta=\rho v^{(0)}$ is the volume fraction where ρ is the number density of the particles and $v^{(0)}$ is their individual volume. The lines denote the coexisting volume fractions at the first-order isotropic-nematic transition as obtained from density-functional theory. The squares and triangles are simulation results for isotropic-nematic and liquid-solid coexistence, respectively. For the former there is good agreement with density-functional theory. The dotted lines are guides for the eye. The isotropic-nematic transition is accompanied by only a small density discontinuity which decreases for $\kappa\to1$. The present density-functional theory is not suited to describe the freezing transition. The simulation data support the symmetry $\kappa\leftrightarrow1/\kappa$ discussed in the text.

lecular volume. The nonpolar case (see Sec. III A and Fig. 1) corresponds to the limit $T^*\to\infty$. For $\kappa=3$ (Fig. 2) the first-order isotropic-nematic transition is shifted to lower densities upon lowering the temperature. Below $T^*\approx0.2$ the density gap increases dramatically and evolves into a broad coexistence region between an isotropic gas and a nematic liquid. Thus in this fluid gas-liquid coexistence is not terminated by a critical point. For $\eta\geqslant0.265$ lowering the temperature leads to two phase transitions (isotropic fluid→nematic fluid and nematic fluid→gas-liquid) whereas for $\eta\leqslant0.265$ there is only the gas-liquid transition. As shown in Fig. 3 for $\kappa=2$ a

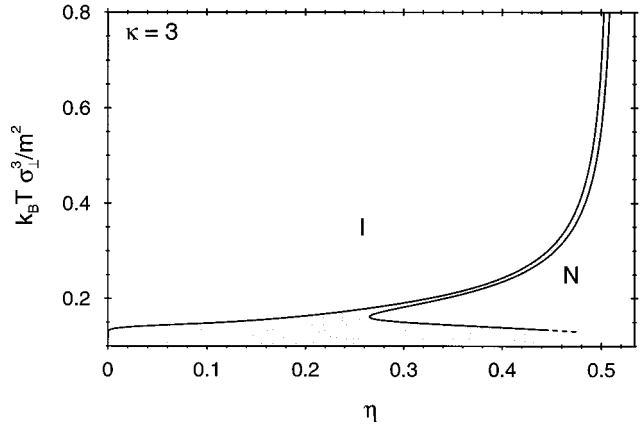

FIG. 2. Phase diagram of dipolar hard ellipsoids with aspect ratio $\kappa=3$ in the temperature-density plane. The weakly first-order isotropic-nematic transition at high temperatures broadens into gas-nematic coexistence at low temperatures. Here and in the following figures two-phase coexistence regions are shaded.

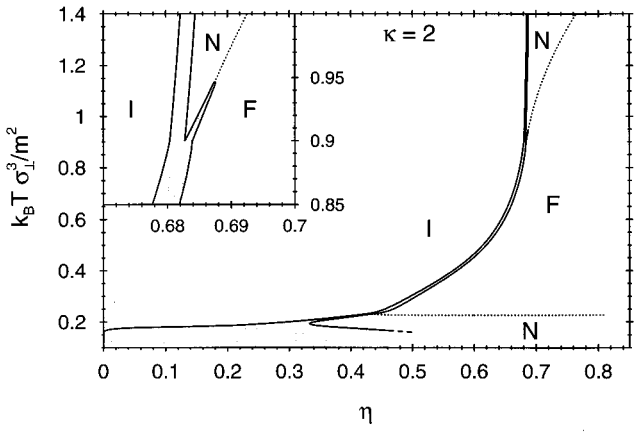

FIG. 3. The same as in Fig. 2 but for $\kappa=2$. Besides the isotropic (I) and nematic (N) phases a ferromagnetically ordered liquid (F) occurs in the intermediate temperature range. The dotted and solid lines denote second- and first-order transitions, respectively. The density gap of the I-N transition at $\eta\simeq0.68$ cannot be resolved on the present scale. The continuous F-N transition at low temperatures intersects the first-order transitions at a critical end point. The inset shows that in a narrow temperature range the high-temperature continuous N-F transition is turned into a weakly first-order transition generating a tricritical point and an I-N-F triple point. The two-phase coexistence regions are shaded. For reasons of clarity this shading is omitted for I-F coexistence.

ferromagnetic liquid appears in the medium-temperature range. This phase turns into a purely nematic phase along the dotted lines of critical points. Whether the disappearence of the ferromagnetic order at low temperatures is an artefact of the approximations or not needs to be checked by alternative techniques. The behavior of the order parameters α_l along different thermodynamic paths is displayed in Figs. 4 and 5. Figure 4 illustrates their density dependence along two isotherms. For $T^*=1.3$ the ferromagnetic order parameter α_1 vanishes at the critical density with a square root singularity in accordance with the presently used mean-field theory while the nematic order parameter α_2 exhibits a small break of slope not visible on the scale of the figure. At a lower

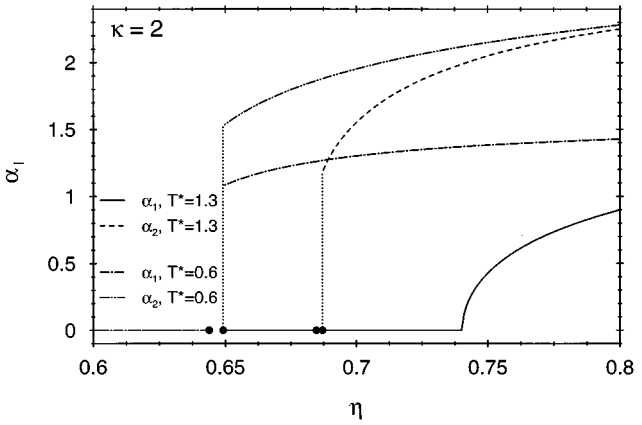

FIG. 4. The first two orientational order parameters α_l [see Eq. (11)] along two isotherms in Fig. 3 for $\kappa=2$. The gaps between the black dots indicate two-phase regions. The dotted vertical lines indicate discontinuities.

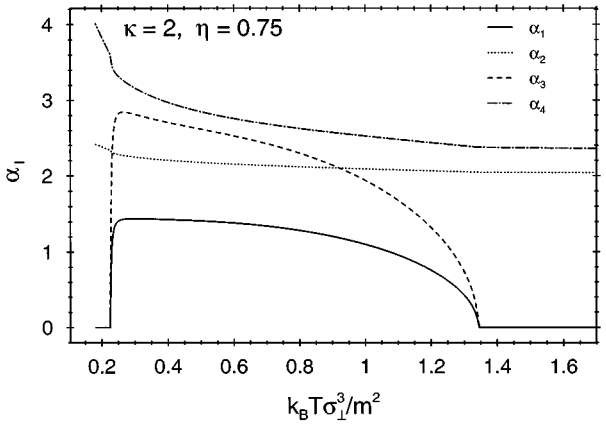

FIG. 5. Temperature dependence of the first four orientational order parameters α_l along a thermodynamic path of fixed density in Fig. 3 for $\kappa=2$. The order parameters with odd indices l vanish in the low- and high-temperature nematic phases but are nonzero between the lower critical point $T^*_{c1}=0.226$ and the upper critical point $T^*_{c2}=1.34$ corresponding to ferromagnetic order. α_2 and α_4 are nonzero for all temperatures and decrease for increasing temperature. At T^*_{c1} and T^*_{c2} they exhibit a break of slope.

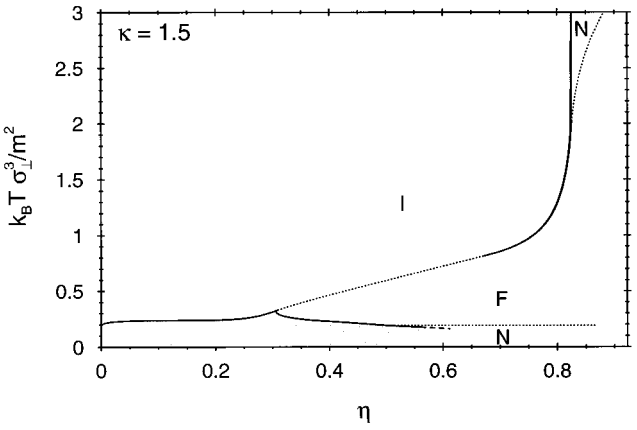

FIG. 6. Phase diagram of dipolar hard ellipsoids for $\kappa=1.5$. The line styles have the same meaning as in Fig. 3. In the high-temperature region the gap between the two coexisting densities cannot be resolved on the scale of the figure so that only a single solid line is visible. Between two tricritical points the isotropic-ferromagnetic transition is continuous. The two-phase coexistence region at low temperatures is shaded.

density α_2 vanishes discontinuously at the first-order nematic-isotropic transition. For the lower temperature $T^*=0.6$ the ferromagnetic phase transforms directly into the isotropic phase. Figure 5 shows the order parameters as function of T^* at the fixed density $\eta=0.75$ demonstrating the loss of the ferromagnetic order at low temperatures. In the intermediate ferromagnetic region the orientational distribution $\overline{\alpha}(\cos\theta)$ typically exhibits two maxima at $\theta=0$ and $\theta=\pi$ with the higher one determining the sign of the spontaneous magnetization. Their heights become equal at the nematic-ferromagnetic transition. In contrast to Baus and Colot [24], who use a different density-functional theory, we do not observe a phase transition between phases with one and two maxima in the orientational distribution.

Upon further lowering the aspect ratio (Fig. 6) another qualitative change of the phase diagram occurs: for intermediate densities the isotropic-ferromagnetic transition becomes continuous. Two tricritical points arise where the character of this transition changes from first to second order. We remark that for high temperatures the ordered phases occur only at such high densities that they will certainly be preempted by a solid phase, which is not captured by the present form of the density functional.

Finally, in Fig. 7 we present the phase diagram for dipolar hard *spheres* obtained from the present density-functional theory. There is no gas-liquid transition between isotropic fluids, but a coexistence of an isotropic gas with a ferromagnetic liquid which at a tricritical point $(T^*_t,\eta_t)=(0.600,0.198)$ changes into a continuous transition. As for the Stockmayer fluid [20] the stability of the ferromagnetic phase is considerably overestimated as compared with simulations [14,15], in which the isotropic-ferromagnetic transition has been detected at $T^*=0.16$ and $\eta\approx0.4$.

For oblate particles ($\kappa<1$) we obtain a similar series of phase diagrams (Figs. 8 and 9) as for $\kappa>1$ but without the loss of ferromagnetic order and the reentrance of the nematic phase at low temperatures. The comparison between Figs. 8 and 6 and between Figs. 9 and 2 shows that the formation of the ferromagnetic phase is favored by oblate particles as compared with elongated ones. This is confirmed in Fig. 10, which displays the phase diagram in the (κ,η) plane for a fixed value of the squared dipole moment per k_BT normalized to the particle volume: $\beta m^2/v^{(0)}=6/\pi$. The isotropic-ferromagnetic critical density increases with increasing elongations. An intuitive explanation for this observation is provided by an examination of the lowest energy configuration of two dipolar particles. The interaction energy at contact of a nose-to-tail arrangement is $-2m^2/(\kappa\sigma_\perp)^3$ while that of an antiparallel side-by-side arrangement is $-m^2/\sigma_\perp^3$. Obviously the former configuration becomes more favorable as compared with the latter one if κ is decreased implying a stronger tendency for long-ranged ferromagnetic order. For large elongations the orientationally ordered phase becomes nematic, while this does not happen for very oblate particles, for which instead a gas-ferromagnetic coexistence occurs at

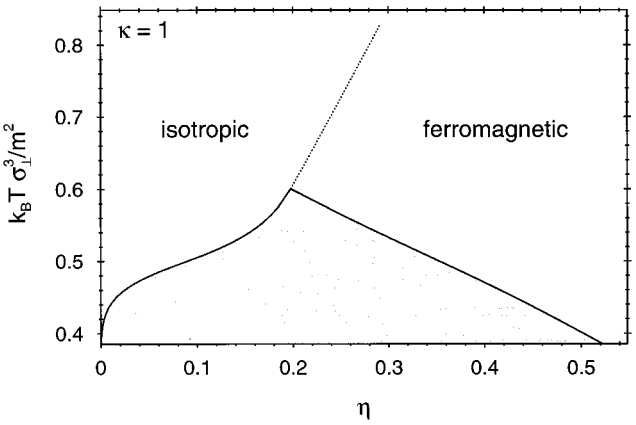

FIG. 7. Phase diagram of dipolar hard spheres. Within the present approximation only one isotropic fluid and a ferromagnetic liquid are stable at any temperature. Below (above) the tricritical point the phase transition is discontinuous (continuous).

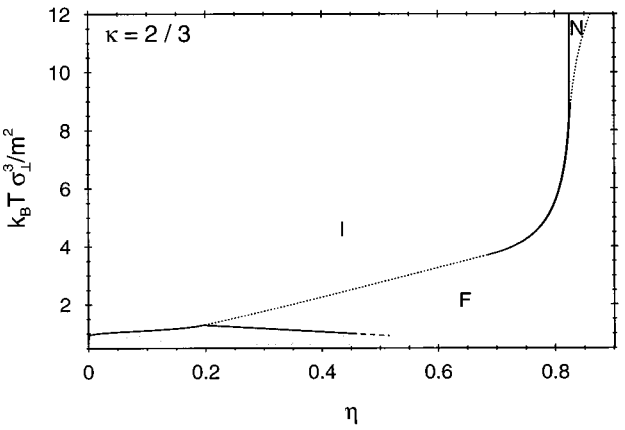

FIG. 8. Phase diagram of oblate dipolar ellipsoids with $\kappa=2/3$. The meaning of the solid and dotted lines is the same as in Fig. 3. In contrast to Fig. 6, there is no reentrant nematic phase at low temperatures.

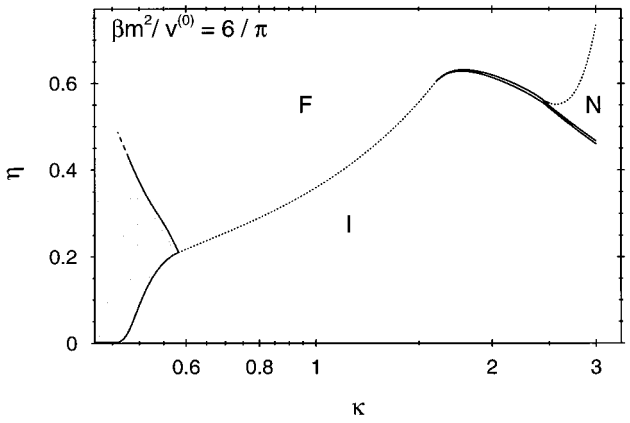

FIG. 10. Phase diagram of hard ellipsoids for a fixed reduced dipole moment in units of k_BT and the particle volume $v^{(0)}$. The stability of the ferromagnetic phase decreases with increasing aspect ratio κ until it finally turns into a nematic phase at high densities and into an isotropic fluid at low densities. Coexistence of an isotropic gas and the ferromagnetic liquid occurs for oblate particles. There is no $\kappa\leftrightarrow 1/\kappa$ symmetry as in Fig. 1 due to the presence of the dipolar interactions.

the temperature considered. Thus the $\kappa\leftrightarrow 1/\kappa$ symmetry of Fig. 1 is lost in Fig. 10 as a result of the additional dipolar forces.

C. Dipolar spherocylinders

For dipolar *spherocylinders* one finds the same series of phase diagrams as function of the aspect ratio L/D as for elongated ellipsoids. An example is given in Fig. 11 (compare Fig. 3). As for the nonpolar ellipsoids the location of the isotropic-nematic transition for $m=0$ agrees very well with corresponding simulation results [6,8], which are available only for $L/D=5$.

D. Comparison with previous results

In the following we compare our results with other theoretical investigations and numerical simulations of dipolar hard core particles. Baus and Colot [24] have studied this problem with a different density-functional ansatz which utilizes the analytically known correlation function of dipolar hard spheres in the mean-spherical approximation. At high temperatures they also find the sequence of isotropic, nematic, and ferromagnetic phases in accordance with our results, followed by a transition to a second ferromagnetic phase (see the end of the first paragraph in Sec. III B). However, they claim that an increase of the aspect ratio shifts the ferromagnetic phase to lower densities and higher temperatures in contrast to our findings and to the qualitative argument presented at the end of Sec. III B.

The familiar second-order virial expansion of Onsager [1] has been applied to dipolar spherocylinders by Vanakaras and Photinos [22]. It is well known that this approximation deteriorates for decreasing aspect ratios [34], which is the reason that for $L/D=5$ and $m=0$ these authors find the isotropic-nematic transition at densities above the density of closest packing. In addition, they do not treat the long-ranged dipolar interactions correctly which leads them to the wrong conclusion that a ferromagnetic phase cannot be stable for any dipole moment or aspect ratio. They agree with our results in that an increase of m or a decrease of T lowers the

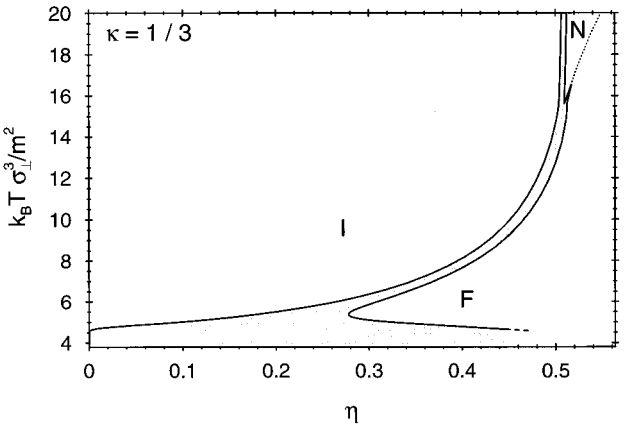

FIG. 9. Phase diagram for oblate dipolar ellipsoids with $\kappa=1/3$. See also the caption to Fig. 3.

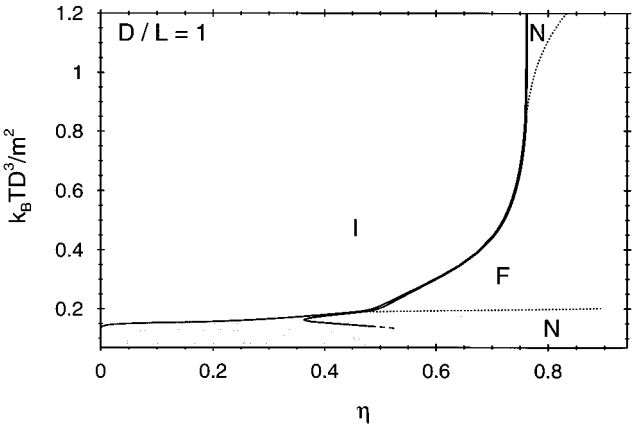

FIG. 11. The phase diagram for polar spherocylinders with an aspect ratio $D/L=1$ exhibits a similar behavior as that for polar ellipsoids with $\kappa=2$ (see Fig. 3).

isotropic-nematic coexistence densities for point dipoles located in the center of the hard particles. However, as they point out, this trend is reversed if the point dipoles are located off center near the ends of the particles.

The correlation functions obtained from the hypernetted-chain integral equation theory have been used by Perera and Patey [23] for the investigation of dipolar hard ellipsoids. For $\kappa=3$ they find transition densities which are about 20% lower than the ones presented here and the same behavior of these densities upon increasing the dipolar strength. However, for $\kappa=1/3$ these authors were able to obtain a solution of the integral equation only for rather small dipole moments. They, too, did not take into account the correct long-ranged contribution to the free energy and did not detect a ferromagnetic phase for the aspect ratios under consideration. However, in a subsequent publication [18] they state that this conclusion remains unaltered if this fault is corrected.

Vega and Lago [25] have used a density-functional theory similar to the present one, but they incorporate a more sophisticated equation of state for the nonpolar isotropic fluid and treat the dipolar interactions within perturbation theory. The same remark as above concerning the treatment of the long-ranged interaction applies also to their work. Their results for the isotropic-nematic coexistence densities of dipolar hard spherocylinders with aspect ratio $L/D=5$ are in fair agreement with our findings for $\beta m^2/D^3$ between 0 and 4. However, they were unable to find a solution for the orientational distribution function for $\beta m^2/D^3=6$, which is close to the parameter range where within our approximation the isotropic-nematic transition broadens into a gas-nematic coexistence.

Weis, Levesque, and Zarragoicoechea [27,28,14] have performed Monte Carlo simulations of dipolar spherocylinders with $L/D=5$ for centered and off-centered dipole moments forming different angles with the cylinder axis. These authors were mainly interested in the structure of the smectic phase and did not determine the isotropic-nematic transition point. For $(\beta m^2/D^3)^{1/2}=2.449$ and a longitudinal centered dipole moment they report [27] the occurrence of an *isotropic* state at $\eta=0.356$ and a *nematic* state at $\eta=0.441$, which is in accordance with the coexistence densities $\eta_I=0.356$ and $\eta_N=0.375$ obtained from the present theory. These authors have also studied ellipsoids with $\kappa=3$ [26] and found no isotropic-nematic transition for values of $(\beta m^2/\sigma_\perp^3)^{1/2}$ in the range between 0 and 3, in contrast to our results shown in Fig. 2. For $m=0$ this finding is also at variance with Frenkel and Mulder's results [5], who did observe an isotropic-nematic transition with $\eta_I=0.507$ and $\eta_N=0.517$. We conclude that further simulations of the isotropic-nematic or possibly the isotropic-ferromagnetic transition for different aspect ratios would certainly be helpful.

Recently, McGrother and Jackson [44] have published an extensive Monte Carlo study of the liquid-vapor coexistence in a dipolar hard spherocylinder fluid. In agreement with previous work [45,17] they find that there is no liquid-vapor coexistence in the spherical limit $L/D\to 0$ as well as for very elongated particles $L/D\gg 1$ due to the formation of chains of nose-to-tail (small L/D) or side-by-side (large L/D) aggregated particles (see also Ref. [46]). Only in an intermediate range around $L/D=0.25$ phase separation into isotropic gas and liquid does occur. This chain formation is not captured correctly by the present theory, which predicts gas-ferromagnetic or gas-nematic coexistence for all values of L/D.

IV. SUMMARY

By applying density-functional theory for the description of orientational order in dipolar fluids consisting of hard nonspherical particles we have obtained the following main results.

(1) The location of the isotropic-nematic transition of nonpolar hard particles as a function of the aspect ratio has been obtained in good agreement with other theories and simulation results (Fig. 1).

(2) The addition of a longitudinal point dipole at the centers of the particles induces a decrease of the coexisting densities of the isotropic-nematic transition and it leads to gas-nematic coexistence for large values of the dipole moment or at low temperatures (Fig. 2).

(3) There is also a ferromagnetic liquid phase provided the particles are not too elongated and the dipole moment is sufficiently strong. This phase is reached from the nematic or isotropic states by continuous or weakly first-order transitions, depending on the temperature and the particle aspect ratio.

(4) In accordance with the mean-field character of density-functional theory, at the continuous phase transitions (Curie points) the magnetization vanishes according to a square root power law and the nematic order parameter exhibits a small break of slope (Figs. 4 and 5).

(5) Within the present theory the phase diagram of dipolar hard spheres (Fig. 7) comprises an isotropic and a ferromagnetic fluid with first- (second-) order phase transitions at temperatures below (above) a tricritical point.

(6) Oblate particles exhibit a similar phase behavior as elongated ones, but a stronger tendency for the formation of the ferromagnetic phase. In contrast to the nonpolar case the phase diagrams are not approximately symmetric with respect to the transformation $\kappa\leftrightarrow 1/\kappa$, where κ is the aspect ratio of the uniaxial ellipsoidal particles (Fig. 10).

(7) For dipolar hard spherocylinders we find an analogous series of phase diagrams as for elongated ellipsoids.

APPENDIX: CRITICAL DENSITIES

We rewrite these contributions to the free energy in Eq. (24) which depend on the orientational distribution as (here and in the following all integrals over x and x' are to be taken over the interval $[-1,1]$)

$$\frac{\Delta F}{V}=\frac{\rho}{\beta}\int dx\,\overline{\alpha}(x)\ln[2\,\overline{\alpha}(x)]+\frac{1}{2}\rho\int dx\,dx'\,\overline{\alpha}(x)\,\overline{\alpha}(x')K(x,x') \tag{A1}$$

with

$$K(x,x')=\sum_{l=1}^{L}\frac{(2l+1)^2}{2}u_l P_l(x)P_l(x'). \tag{A2}$$

Following van Roij *et al.* [47] we use a kind of bifurcation analysis in order to determine the critical density of the nematic-ferromagnetic or isotropic-ferromagnetic phase transition for a given temperature. The minimization of Eq. (A1) yields

$$\ln[2\overline{\alpha(x)}]+\beta\rho\int dx'\,\overline{\alpha(x')}K(x,x')=\nu, \tag{A3}$$

where the Lagrange multiplier ν is determined by the normalization $\int dx\overline{\alpha(x)}=1$. One considers a small ferromagnetic perturbation $\overline{\alpha_1}(x)$ of a solution $\overline{\alpha_0}(x)$ with nematic symmetry, i.e., $\overline{\alpha_0}(x)=\overline{\alpha_0}(-x)$. If the expansions $\overline{\alpha(x)}=\overline{\alpha_0}(x)+\epsilon\overline{\alpha_1}(x)+\cdots$ and $\nu=\nu_0+\epsilon\nu_1+\cdots$ are inserted into Eq. (A3) the term linear in ϵ gives

$$\frac{\overline{\alpha_1}(x)}{\overline{\alpha_0}(x)}+\beta\rho\int dx'\,\overline{\alpha_1}(x')K(x,x')=\nu_1. \tag{A4}$$

Integrating Eq. (A4) over x and using the relation $\int dxK(x,x')=0$ yields

$$\frac{\overline{\alpha_1}(x)}{\overline{\alpha_0}(x)}-\frac{1}{2}\int dx'\,\frac{\overline{\alpha_1}(x')}{\overline{\alpha_0}(x')}+\beta\rho\int dx'\,\overline{\alpha_1}(x')K(x,x')=0. \tag{A5}$$

Since both $\overline{\alpha_0}(x)$ and $\overline{\alpha(x)}$ must be of the form $\exp[\Sigma_{l=0}^{L}\gamma_l P_l(x)]$ [see Eq. (26)], with the nematic solution $\overline{\alpha_0}(x)$ containing only even indices l, we make the following ansatz for the small perturbation:

$$\overline{\alpha_1}(x)=\overline{\alpha_0}(x)\sum_{n=1}^{L/2}\gamma_{2n-1}P_{2n-1}(x), \tag{A6}$$

where terms of the order $\gamma_{2n-1}\gamma_{2m-1}$ and higher due to the exponential form (see above) have been neglected. Due to Eq. (A5) the coefficients γ_l with odd l satisfy the equation

$$\gamma_l+\sum_{l'=1}^{L/2}A_{ll'}\gamma_{l'}=0, \tag{A7}$$

with

$$A_{ll'}=\frac{(2l+1)^2}{2}\beta\rho u_l\int dx\,\overline{\alpha_0}(x)P_l(x)P_{l'}(x). \tag{A8}$$

Both the nematic solution $\overline{\alpha_0}(x)$ and the $L/2\times L/2$ matrix A depend on the density. The critical density is reached if one of the eigenvalues of A equals -1 giving rise to a nontrivial solution of Eq. (A7). For $L=2$ this condition reduces to

$$\tfrac{9}{2}\beta\rho u_1\int dx\,\overline{\alpha_0}(x)x^2=-1. \tag{A9}$$

For $L=4$ one obtains after some algebra

$$1+A_{11}+A_{33}+A_{11}A_{33}-A_{13}A_{31}=0. \tag{A10}$$

From these equations together with the numerical solution of Eq. (27) the nematic-ferromagnetic critical density can be determined.

For the isotropic-ferromagnetic transition the unperturbed solution is $\overline{\alpha_0}(x)=1/2$ so that Eq. (A9) reduces to the known result [see Eq. (7.10) in Ref. [20]]

$$\tfrac{3}{2}\beta\rho u_1=-1. \tag{A11}$$

In this case the matrix A is diagonal for general L: $A_{ll'}=(2l+1)/2\beta\rho u_l\delta_{l,l'}$. Thus the above bifurcation condition yields

$$\frac{2l+1}{2}\beta\rho u_l=-1. \tag{A12}$$

The actual values of the coefficients u_l are such that the lowest density for which Eq. (A12) is satisfied always corresponds to $l=1$, so that Eq. (A11) is valid for all L.

[1] L. Onsager, Proc. N.Y. Acad. Sci. **51**, 627 (1949).
[2] D. Frenkel, in *Les Houches Summer School Lectures, Session LI*, edited by J.P. Hansen, D. Levesque, and J. Zinn-Justin (Elsevier, Amsterdam, 1991), p. 689.
[3] P. Tarazona, Philos. Trans. R. Soc. London A **344**, 307 (1993).
[4] M.P. Allen, G.T. Evans, D. Frenkel, and B.M. Mulder, Adv. Chem. Phys. **86**, 1 (1993).
[5] D. Frenkel and B.M. Mulder, Mol. Phys. **55**, 1171 (1985).
[6] D. Frenkel, H.N.W. Lekkerkerker, and A. Stroobants, Nature **332**, 822 (1988).
[7] D. Frenkel, J. Phys. Chem. **92**, 3280 (1988).
[8] J.A.C. Veerman and D. Frenkel, Phys. Rev. A **41**, 3237 (1990).
[9] S.C. McGrother, D.C. Williamson, and G. Jackson, J. Chem. Phys. **104**, 6755 (1996).
[10] D. Frenkel, Liq. Cryst. **5**, 929 (1989).
[11] J.A.C. Veerman and D. Frenkel, Phys. Rev. A **45**, 5633 (1992).
[12] D. Wei and G.N. Patey, Phys. Rev. Lett. **68**, 2043 (1992).
[13] D. Wei and G.N. Patey, Phys. Rev. A **46**, 7783 (1992).
[14] J.J. Weis, D. Levesque, and G.J. Zarragoicoechea, Phys. Rev. Lett. **69**, 913 (1992).
[15] J.J. Weis and D. Levesque, Phys. Rev. E **48**, 3728 (1993).
[16] M.J. Stevens and G.S. Grest, Phys. Rev. E **51**, 5962 (1995).
[17] M.J. Stevens and G.S. Grest, Phys. Rev. E **51**, 5976 (1995).
[18] D. Wei, G.N. Patey, and A. Perera, Phys. Rev. E **47**, 506 (1993).
[19] B. Groh and S. Dietrich, Phys. Rev. Lett. **72**, 2422 (1994); **74**, 2617 (1995).
[20] B. Groh and S. Dietrich, Phys. Rev. E **50**, 3814 (1994).
[21] B. Groh and S. Dietrich, Phys. Rev. E **53**, 2509 (1996).
[22] A.G. Vanakaras and D.J. Photinos, Mol. Phys. **85**, 1089 (1995).

[23] A. Perera and G.N. Patey, J. Chem. Phys. **91**, 3045 (1989).
[24] M. Baus and J.-L. Colot, Phys. Rev. A **40**, 5444 (1989).
[25] C. Vega and S. Lago, J. Chem. Phys. **100**, 6727 (1994).
[26] G.J. Zarragoicoechea, D. Levesque, and J.J. Weis, Mol. Phys. **75**, 989 (1992).
[27] J.J. Weis, D. Levesque, and G.J. Zarragoicoechea, Mol. Phys. **80**, 1077 (1993).
[28] D. Levesque, J.J. Weis, and G.J. Zarragoicoechea, Phys. Rev. E **47**, 496 (1993).
[29] K. Satoh, S. Mita, and S. Kondo, Liq. Cryst. **20**, 757 (1996).
[30] E.M. Terentjev, M.A. Osipov, and T.J. Sluckin, J. Phys. A **27**, 7047 (1994).
[31] J.-L. Colot, X.-G. Wu, H. Xu, and M. Baus, Phys. Rev. A **38**, 2022 (1988).
[32] R. Pynn, Solid State Commun. **14**, 29 (1974); J. Chem. Phys. **60**, 4579 (1974).
[33] J.P. Hansen and I.R. MacDonald, *Theory of Simple Liquids*, 2nd ed. (Academic, London, 1986).
[34] S.-D. Lee, J. Chem. Phys. **87**, 4972 (1987).
[35] S.-D. Lee, J. Chem. Phys. **89**, 7036 (1988).
[36] N.F. Carnahan and K.E. Starling, J. Chem. Phys. **51**, 635 (1969).
[37] P.I. Teixeira and M.M. Telo da Gama, J. Phys. Condens. Matter **3**, 111 (1991).
[38] P. Frodl and S. Dietrich, Phys. Rev. A **45**, 7330 (1992); Phys. Rev. E **48**, 3203 (1993).
[39] J.M. Tavares, M.M. Telo da Gama, P.I.C. Teixeira, J.J. Weis, and M.J.P. Nijmeijer, Phys. Rev. E **52**, 1915 (1995).
[40] R.B. Griffiths, Phys. Rev. **176**, 655 (1968).
[41] S. Chandrasekhar, *Liquid Crystals* (Cambridge University Press, Cambridge, 1992).
[42] B.J. Berne and P. Pechukas, J. Chem. Phys. **56**, 4213 (1972).
[43] B. Groh and S. Dietrich, Phys. Rev. E **54**, 1687 (1996).
[44] S.C. McGrother and G. Jackson, Phys. Rev. Lett. **76**, 4183 (1996).
[45] M.E. van Leeuwen and B. Smit, Phys. Rev. Lett. **71**, 3991 (1993).
[46] R. van Roij, Phys. Rev. Lett. **76**, 3348 (1996).
[47] R. van Roij, P. Bolhuis, B. Mulder, and D. Frenkel, Phys. Rev. E **52**, R1277 (1995).